ARTICLE

Check for updates

Strength and variability of the Oligocene Southern Ocean surface temperature gradient

Frida S. Hoem [1✉], Isabel Sauermilch[1], Adam K. Aleksinski[2], Matthew Huber[2], Francien Peterse [1], Francesca Sangiorgi [1] & Peter K. Bijl[1]

Large Oligocene Antarctic ice sheets co-existed with warm proximal waters offshore Wilkes Land. Here we provide a broader Southern Ocean perspective to such warmth by reconstructing the strength and variability of the Oligocene Australian-Antarctic latitudinal sea surface temperature gradient. Our Oligocene TEX_{86}-based sea surface temperature record from offshore southern Australia shows temperate (20–29 °C) conditions throughout, despite northward tectonic drift. A persistent sea surface temperature gradient (~5–10 °C) exists between Australia and Antarctica, which increases during glacial intervals. The sea surface temperature gradient increases from ~26 Ma, due to Antarctic-proximal cooling. Meanwhile, benthic foraminiferal oxygen isotope decline indicates ice loss/deep-sea warming. These contrasting patterns are difficult to explain by greenhouse gas forcing alone. Timing of the sea surface temperature cooling coincides with deepening of Drake Passage and matches results of ocean model experiments that demonstrate that Drake Passage opening cools Antarctic proximal waters. We conclude that Drake Passage deepening cooled Antarctic coasts which enhanced thermal isolation of Antarctica.

[1] Department of Earth Sciences, Utrecht University, Utrecht, The Netherlands. [2] Department of Earth, Atmospheric and Planetary Sciences, Purdue University, West Lafayette, IN, USA. ✉email: Frida.snho@gmail.com

Southern high-latitude sea surface temperature (SST) records from the Oligocene (33.9–23.0 Ma)[1–4] show unexpectedly warm-temperate conditions, despite evidence for the coeval presence of a large Antarctic ice sheet[5], which extended to the margins of the continent[6–8]. This apparent contradiction requires reconciliation[9]. A warm Oligocene Southern Ocean could be the result of generally high atmospheric pCO_2 concentrations (300–700 parts per million (ppm); https://www.paleo-co2.org[10]), but higher pCO_2 would also typically be associated with reduced ice volume[11]. Furthermore, since enhanced Antarctic ice volume should have cooled marginal seas[12] the mystery of warm high-latitude SSTs and greater ice volume grows. One alternative hypothesis is that marine ice sheet terminations were restricted to the southernmost parts of the Antarctic margin, facilitated by a higher-than-modern Antarctic paleotopography[13,14], while elsewhere the ice sheets were mostly terrestrial (e.g., refs. [15,16]), limiting the Antarctic glacial cooling effect on proximal SSTs[17]. Or as a final hypothesis, critical Southern Ocean gateways (Tasmanian Gateway and Drake Passage) may have played a role in ocean heat redistribution[18]. Closed ocean gateways, could reduce the meridional temperature gradients by enhancing ocean poleward heat transport or by increasing local radiative heating through albedo feedbacks, but might also have enhanced the atmospheric moisture transport[2,19,20], thereby potentially maintaining terrestrial ice sheets. Each of these factors (radiative forcing, ice sheet configuration and tectonic changes) would have had a unique spatial fingerprint of Southern Ocean SST changes relative to those at the Antarctic continental margin and unravelling the complexities is challenging. Atmospheric pCO_2-associated radiative forcing would be expected to cause globally synchronous temperature trends on both long- and orbital-time scales, although with a degree of polar amplification. Ice sheet growth increase poleward heat transport[21], but at the same time induces local cooling at the Antarctic margin[12]. The different response to Antarctic glaciation in different model experiments (Supplementary Table 1) can be attributed to subtle changes in paleogeography and model set-up[22]. In any case, ice volume change has the most effect close to the Antarctic continent, and is further evident in benthic foraminiferal $\delta^{18}O$[23] and deep-sea cooling[24]. Finally, opening of gateways would result in profound cooling of Antarctic proximal waters[25,26] while leaving the rest of the world's sea surface temperatures largely unaffected[12,19]. Although the Antarctic proximal cooling could result in deep-sea cooling[27], which would redistribute globally, the question remains how strong the resulting global cooling would be. Thus, as opposed to ice volume changes, gateway opening cause a step-wise, unidirectional change in temperature: changes in SSTs could then be stratigraphically linked to phases of gateway opening[25,28]. Currently, Oligocene SST records from the subtropics are lacking, which hinders establishing the latitudinal SST gradients needed to provide context for ice-proximal SST changes, and to evaluate the possible factors that drove the development of Oligocene Southern Ocean surface conditions.

Here, we present TEX_{86}-based SST estimates from Late Eocene–Early Miocene ODP Site 1168 sediments, 339–765 meters below sea floor (mbsf), west of Tasmania (red dot in Fig. 1). To explore the development of the Oligocene SST gradient across the Tasmanian Gateway region, we compared our data with TEX_{86} based SSTs from east of Tasmania (ODP Site 1172)[29], west of the Campbell Plateau (DSDP Site 277)[4], north of the Ross Sea (DSDP Site 274)[2], offshore Wilkes Land (IODP Site U1356[1] and DSDP Site 269[30]) and inorganic chemical weathering indices recording terrestrial temperature from the Cape Roberts Project (CRP) in the Ross Sea[31] (Fig. 1). As most of these records cannot be resolved at orbital, glacial-interglacial variability, we predominantly discuss long-term relative SST trends and the
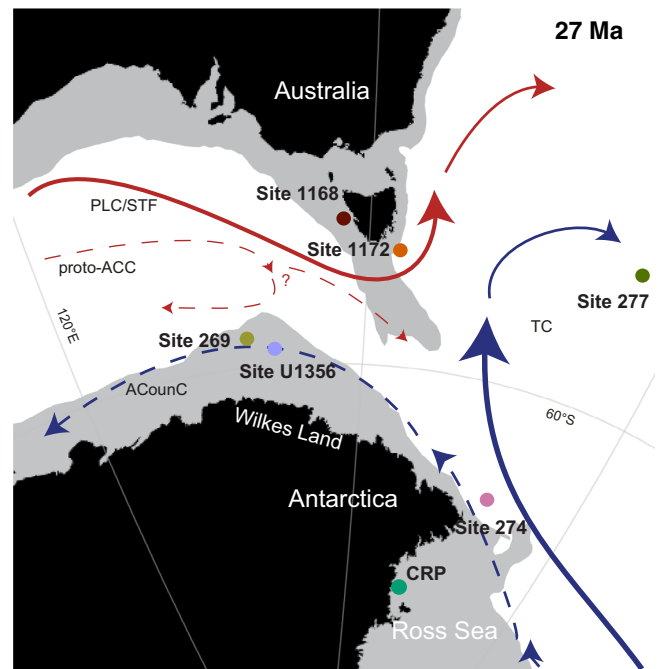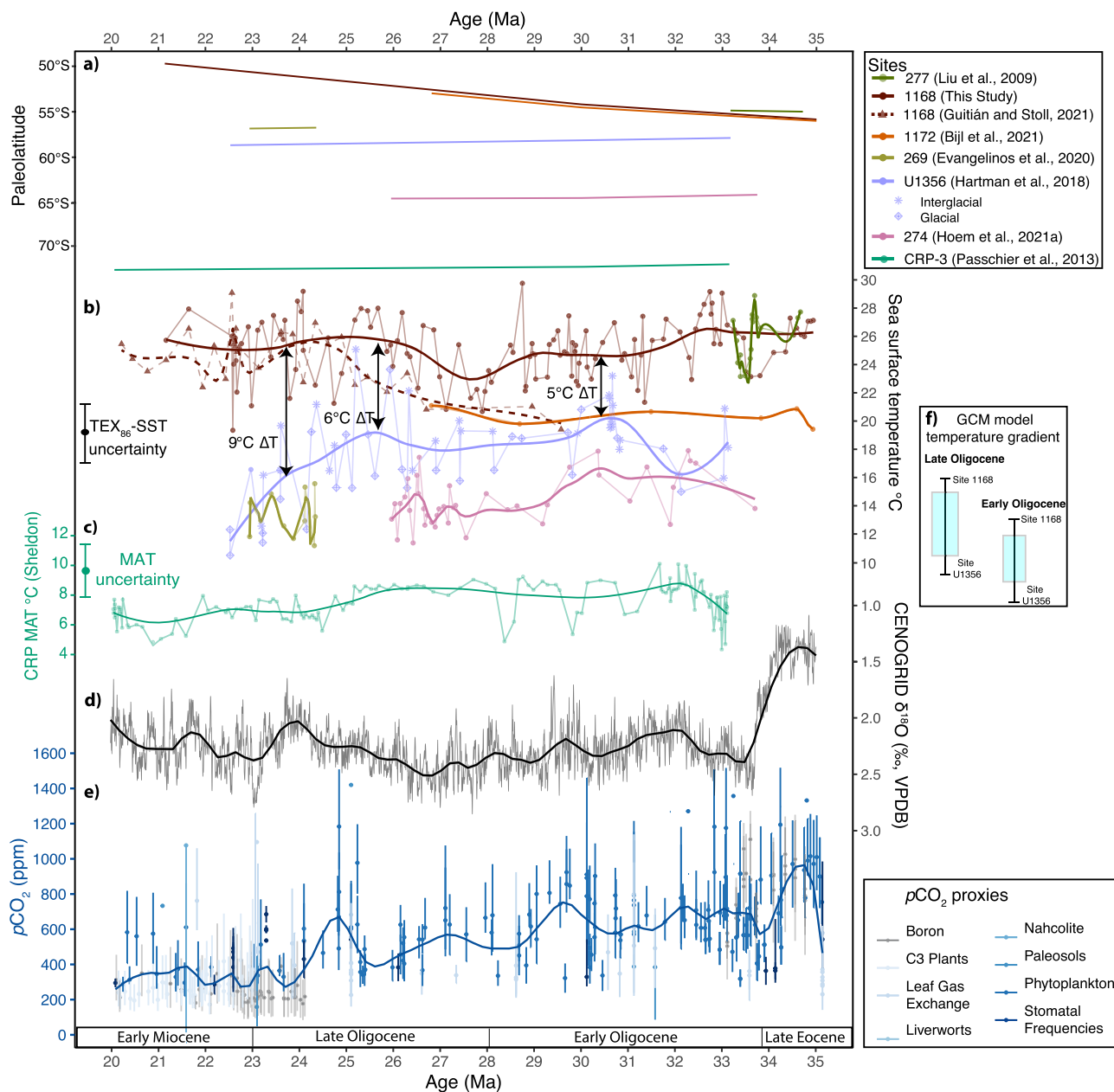

Fig. 1 Paleogeographic map of the Oligocene locations of study sites and prevailing ocean currents. The approximate paleogeography at 27 Ma is reconstructed through G-plates (http://www.gplates.org), based on the global geodynamic rotation model from Müller, et al.[70]. Black represents the outline of modern coastlines. The grey outline corresponds to the modern 2000 m water depth contour. PLC Proto-Leeuwin Current, STF Subtropical front, TC Tasman Current, proto-ACC proto-Antarctic Circumpolar Current and ACountC=Antarctic counter current (after Houben, et al.[3]).

amplitude of variability. These SST records are compared to the temperature distribution in a coarse-resolution (3° horizontal), fully coupled general circulation model (GCM, following Kennedy-Asser, et al.[26] HadCM3L – Hadley Centre Coupled Model), which simulates equilibrium temperature response to CO_2 forcing, and the role of ice volume and geographic boundary conditions of the Early- and Late Oligocene (33.9–28.1, 28.1–23 Ma). Details of ocean heat transport and consequences of local bathymetry are subsequently investigated by comparing SST results to high horizontal resolution (0.25°) ocean-only model simulations[25]. Our results show an increase in the SST gradient across the Southern Ocean starting at 26 Ma, when Antarctic-proximal SSTs cooled. This is in contrast to a synchronous decrease in global benthic foraminiferal $\delta^{18}O$ indicating ice mass loss/deep sea warming. Considering the potential drivers of such cooling, we conclude that the Late Oligocene Antarctic-proximal SST cooling is not primarily driven by changes in pCO_2 and ice sheet configuration, but by paleogeographic configurations.

Results

Our SST record is based on 148 samples from ODP Site 1168 which were processed for TEX_{86} paleothermometry. Twenty-two showed potential for non-thermal overprints, thereby considered unreliable, and discarded from the dataset (see Supplementary Information). Results indicate Late Eocene–Early Miocene (35–20 Ma; red line Fig. 2b; Supplementary Data[32]) SSTs of 20–29 °C (± 4 °C standard calibration error). The amplitude of SST variability was high (5–7 °C) around 28 Ma and from 25 Ma onwards, and low (~3 °C) between 32–29 Ma and 27–25 Ma. Our record indicates 4 °C cooling (from 27 to 23 °C) across the Eocene–Oligocene transition (ca. 34 Ma) and then a return to high temperatures of ~29 °C at

Fig. 2 Late Eocene–Early Miocene Australian-Antarctic Gulf temperature records, with their paleolatitude, compared with global benthic δ¹⁸O and pCO₂ records and GCM models. a Paleolatitude evolution of sites[65]. Colors refer to sites in Fig. 1. **b** TEX₈₆- SST reconstructions. Thick lines represent smoothed long-term trends, with a local weighted polynomial regression (LOESS; span of 0.35). For the age model of Site 1168 see Supplementary Data[32]. **c** Mean annual air temperature (MAT) from Site CRP-3[31]. All ages in a–c are converted to GTS2012[51]. **d** Benthic foraminiferal δ¹⁸O splice, smoothed by a locally weighted function over 20 kyr (thin black curve; CENOGRID[23]). Thick black curve is the LOESS smoothed (span = 0.1). **e** paleo-CO₂ compilation from https://www.paleo-co2.org[10]. The vertical error bars indicate the 95% confidence interval for each pCO₂ estimate. Blue curve is the LOESS smoothed (span = 0.1). **f** Shows the GCM model temperature gradient (corresponding to the scale in b) between Site 1168 and Site U1356 in the Early- and Late Oligocene.

33.2 Ma. Temperatures then gradually cooled until ~28 Ma. A transient warming of 6 °C occurred from 27.8–24.3 Ma, followed by a gradual cooling from 24.3–22.2 Ma. The TEX₈₆-based SSTs are generally warm and in line with U$^{k'}_{37}$-based SSTs of 19 °C to 29 °C derived from the same records for the 29.8–16.7 Ma interval[33] (Supplementary Fig. 7). The U$^{k'}_{37}$-based SST record shows a more prominent Late Oligocene warming, although U$^{k'}_{37}$-based SSTs remains within the variability of the TEX₈₆-based SST record (stippled line Fig. 2b). The discrepancy between TEX₈₆ and U$^{K}_{37}$ could be explained by difference in the season or in the water depth where the proxies are produced (e.g. Herbert et al.,[34]). Yet, a

prominent input of deep-dwelling archaeal GDGTs at this site is unlikely, as the GDGT2/3 ratios are low[35,36] (<5; Supplementary Fig. 3f). Moreover, SST derived by TEX₈₆ proxy are warmer than those from U$^{K'}_{37}$. With a substantial contribution from deep-dwelling archaea, a cold-bias in TEX₈₆ would be expected because the photic zone requirement of alkenone producers makes U$^{K'}_{37}$ a proxy for SST, while GDGT producers occur also below the photic zone. This lends confidence that the TEX₈₆ proxy reflects SST at this site. Further support for the warm-temperate SSTs comes from dinoflagellate cyst (dinocyst) assemblages analyzed on the same samples[37].
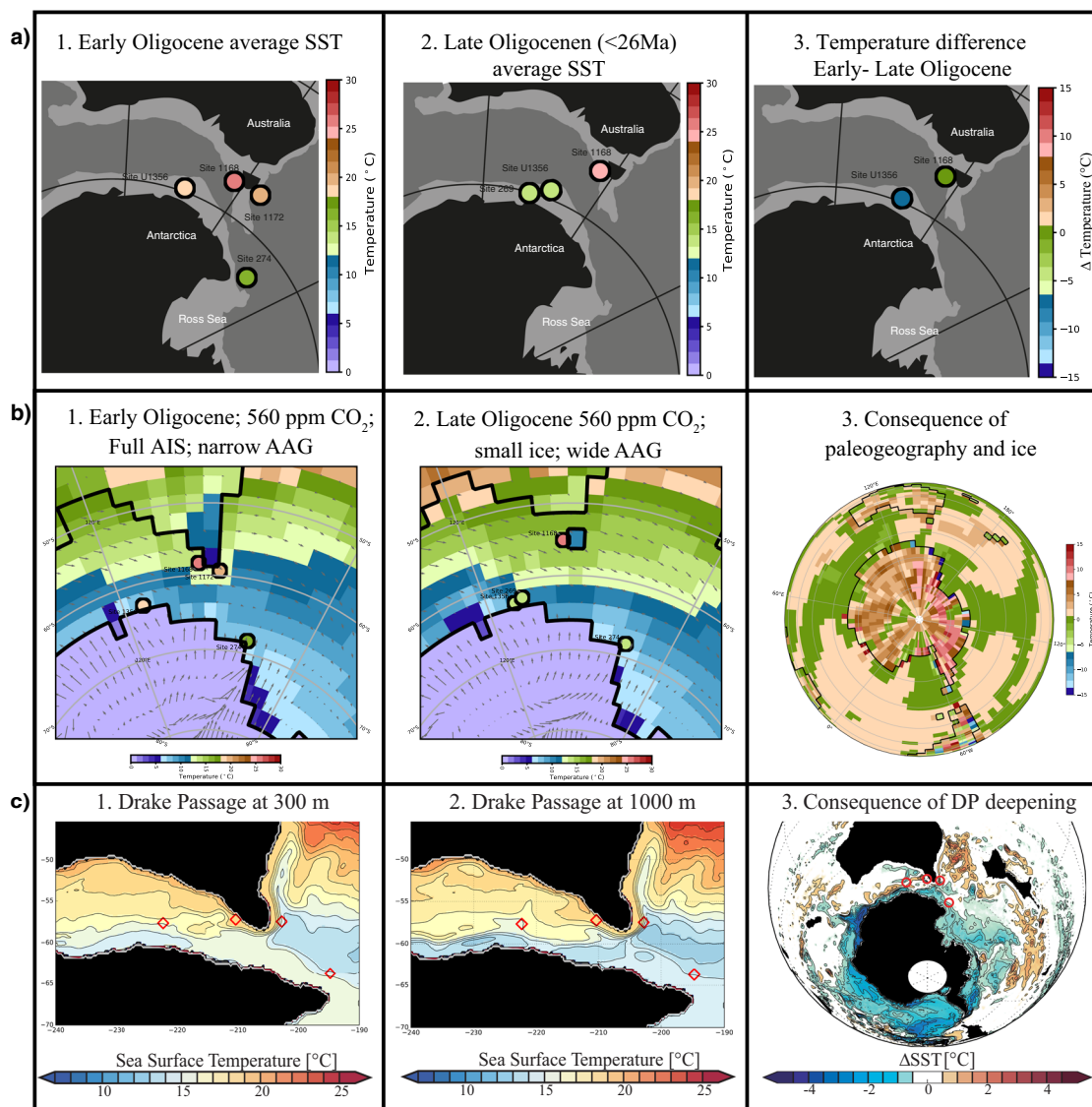
Fig. 3 Data-model experiment comparisons. a Paleogeographic map with SST data shown in colored dots from the respective drill sites. **b** Modeled SSTs from fully coupled HadCM3L simulations of the Early-(33.9–28.4 Ma) and Late Oligocene (28.4–23.0 Ma)[26]. The modeled simulations are TDLUQ and TDLUP respectively (see Supplementary Table 2). TDLUP SSTs are differenced from TDLUQ SSTs in the third panel. **c** High-resolution ocean model[25]. The Southern Ocean paleogeography is reconstructed for Late Eocene (38 Ma) for all three panels, red circles indicate the studied sites.

Discussion

Temperature gradient across the Australian-Antarctic Gulf. We focus the discussion on the SST gradient across the Australian-Antarctic Gulf (AAG), between Sites 1168 and U1356 in the proxy data compilation (arrows, Fig. 2), due to their high temporal resolution, while Sites 1172, 277, 274 and 269 offer a broader regional context. We note a persistent SST gradient (5–10 °C) between the Antarctic-proximal (Site U1356) and the subtropical (Site 1168) sites, albeit smaller than at present-day (~14 °C)[38]. Still, this implies that (polar) frontal systems separated water masses latitudinally in the Oligocene AAG. The Early Oligocene latitudinal separation of water masses is further corroborated by the strong latitudinal separation in dinocyst assemblages from ~30 Ma onwards between the Australian (Site 1172[3] and 1168[37], relatively oligotrophic) and Antarctic (Site U1356[15], 269[30] and 274[2], eutrophic, upwelling) margins of the AAG.

The reconstructed SST gradient is in line with the output of two Oligocene GCM simulations (Fig. 3b), albeit absolute SSTs are in general lower throughout the region in the model simulations (10–20 °C; Fig. 2, Fig. 3a,b) than in the TEX$_{86}$-based SST records (15–29 °C). This could be the result of a warm bias in

the TEX$_{86}$ proxy (e.g., Hartman et al.[1]), as suggested by the slightly cooler U$^{k'}_{37}$-based SSTs[33] (stippled line Fig. 2b) and/or to too low climate sensitivity in the GCMs. We acknowledge that a cold bias is known to be a persistent issue with the Had3CML GCM as with nearly all GCMs for past warm climate intervals, including in the Oligocene ([9],[39]). The two different ice sheet sizes in the Early- and Late Oligocene simulations can be used to evaluate the effects of variability in ice sheet size as well as the effect of long-term changes in geographic boundary conditions on the simulated latitudinal SST gradient. We do acknowledge that this interpretation derives from a low-resolution model, which poorly represents eddy flow, as no high-resolution ocean models that simulate the oceanographic effect of Antarctic ice sheet size are available. Interestingly, while SST difference derived from sediments deposited during glacial or interglacial intervals from Site U1356 is high[1,15,40] (indicated by separate symbols in Fig. 2b), two different ice sheet sizes in the Early- and Late Oligocene GCM simulations, which also includes a widening of the AAG, are of little (~1 °C) impact to the simulated latitudinal SST gradient (Fig. 3b). We also note that the difference in

Table 1 Scenarios to explain Late Oligocene trends in SST and deep sea δ^{18}O.

Scenario	Antarctic proximal SST	Subtropical SST	Deep ocean δ^{18}O	Evaluation
Observations from the Late Oligocene proxy data	*Cooling*	*Stable/slight warming*	*Decreasing*	*Target*
1. pCO$_2$ decrease	Cooling	Cooling	Increasing	Failure
2. Antarctic Ice Sheet expansion	Cooling	Stable/slight cooling	Increasing	Failure
3. Deepening of oceanic gateways and Antarctic ice loss	Cooling	Stable	Decreasing	Success

amplitude of SST change between offshore Australia and Antarctica is too large to be caused only by greenhouse gas induced radiative forcing with a factor of polar amplification. Therefore, we ascribe the high amplitude temperature signal to shifts in ocean frontal systems. The small effect of the northward tectonic drift of Site 1168 on regional SSTs, indicates that the subtropical front (STF) likely migrated northward along with the Australian landmass, as has been suggested from microfossil data[37]. This effect is further muted at Site 1168, because Australia hinders northward migration of the STF, which explains the smaller temperature swings offshore Australia.

Late Oligocene paleogeographic, ocean temperature, atmospheric pCO$_2$ and ice volume changes. In the Late Oligocene we note the substantially increasing temperature gradient across the AAG latitudinal transect from 6 °C prior to 26 Ma to >9 °C by 23.5 Ma (Fig. 2). This is mostly due to unidirectional progressive cooling of the Antarctic-proximal SST record at Site U1356 and stepwise air temperature cooling at CRP[31] starting at around 26 Ma, opposite to slightly increasing SSTs (U$^{k'}_{37}$-based SST, increasing the most[33]) at Site 1168 and the benthic foraminiferal δ^{18}O splice (CENOGRID[23], Fig. 2d) showing Late Oligocene warming and ice mass loss. We note that the CENOGRID benthic foraminiferal δ^{18}O records are derived from lower latitudes (<30°) in the Atlantic and Pacific, and might therefore not fully be representative for "global" deep-sea temperatures/ice mass. The Antarctic-proximal cooling continues into the Miocene, where the δ^{18}O record also show deep ocean cooling. Meanwhile the subtropical SSTs at Site 1168 show a Late Oligocene warming coincident with trends in δ^{18}O record (Fig. 2d). The slightly cooler Late Oligocene SSTs at Site 269, northeast of Site U1356, have been attributed to its proximal location to upwelling[30], while the cooler SSTs at Site 274 is attributed to its higher latitude and proximity to the colder Ross Sea[2], as also inferred from the air temperature record[31] (Fig. 2c) and fossil record[41] at CRP.

We break down the complex interplay of forcings and feedbacks that kept the Early Oligocene Southern Ocean warm and caused cooling of the Wilkes Land Antarctic Margin at 26 Ma – changes in atmospheric pCO$_2$ levels, ice volume or paleogeography (Table 1). Late Oligocene atmospheric pCO$_2$ gradually decline (700–300 ppm[10]; Fig. 2e), but, the latitudinally contrasting paleotemperature trends, with Antarctic-proximal SSTs cooling, subtropics remaining warm and equatorial areas warming[9], are difficult to attribute primarily to pCO$_2$ as shown in the climate model results (Supplementary Table 2, Supplementary Fig. 8c and f, Supplementary Fig. 9c, f and i). In Community Earth System Model simulations by Goldner et al.[12], the expansion of Antarctic ice sheets generates cooling of 6 °C at the Antarctic margin, while in atmosphere - ocean GCM model simulations by Knorr and Lohmann[21] an expanded ice sheet would cause regional warming at the Antarctic margin (Supplementary Table 1). Nonetheless, an expanding Late Oligocene ice volume is unlikely given the decreasing benthic δ^{18}O indicating loss of Antarctic ice volume with deep-sea warming[23,24], which has been ascribed to local tectonism on Antarctica[13,17]. Duncan et al.[42] recorded the same enigmatic Late Oligocene (25–24 Ma) trend of cooling SSTs at the

Ross Sea and Wilkes Land margins and ice volume loss, which they attributed to the tectonic subsidence of West Antarctica which favored the influx of the still relatively warm ocean waters in the Ross Sea region precluding the advance of a marine-based ice sheet. Although this provides a plausible explanation for the SST and ice volume trends in the Ross Sea, it doesn't explain why Antarctic proximal SSTs cool around the east Antarctic Margin.

Moreover, the Early- and Late Oligocene GCM model results show little effect of AAG widening and ice volume changes on the Southern Ocean SST gradient (Fig. 3b). The Late Oligocene breakdown of the relationship between SST, deep ocean temperature, atmospheric pCO$_2$ and ice volume[9] suggests that Antarctic proximal SST cooling was not limited to pCO$_2$ changes or a glaciation-induced negative feedback[12], but probably also affected by paleogeographic configurations.

Tectonic deepening of Drake Passage caused cooling along Antarctic Margin. Low-resolution coupled climate models have suggested that opening of Southern Ocean gateways had little effect on poleward ocean heat transport and polar climate[12,43]. However, recently, the importance of the high horizontal resolution of ocean model simulations in such experiments has been underlined[19,26]. Eddy-permitting model simulations[25] show that deepening of the second of two Southern Ocean gateways (Drake Passage and Tasmanian Gateway) below 300 m drives surface water cooling at the Antarctic margin (up to 5 °C), while leaving the rest of the Southern Ocean with little relative temperature changes (Fig. 3c). These models are uncoupled so it is currently impossible to know if the same result would obtain if the atmosphere and sea ice could respond and feedback on to this cooling. Although it would be desirable to utilize fully coupled high-resolution models, it is too computationally expensive to run them long enough to verify the deep-ocean response. Despite this modeling limitation, it is compelling that this is exactly what can be seen in the SST compilation at 26 Ma: The SST at the STF remains relatively stable despite northward migration and the Antarctic proximal Site U1356 cools (Fig. 2), while the benthic δ^{18}O records shows apparent global warming/ice loss. The gradual northward migration of Australia could have progressively invited a larger volume of east-flowing STF water to follow the southward route around Australia[18], without changing the absolute temperature in the STF region. This southward route would also progressively line up better with the westerly wind belt, strengthening the proto-Antarctic Circumpolar Current[44,45]. A strengthened proto-Antarctic Circumpolar Current would deflect the warm poleward extension of the subpolar gyres, including the proto-Leeuwin Current away from Antarctica, and reduce heat transport towards Wilkes Land Antarctic Margin, increasing polar isolation[25]. Crucially, the timing of this observed gradient increase coincides with evidence from kinematic reconstructions of Drake Passage[28] showing a first deep ocean connection around 26 Ma. Also, sediments from the South Pacific indicate the formation of the proto-Antarctic Circumpolar Current in the Late Oligocene (ca. 25–23 Ma)[46]. Thus, we deduce that despite proximity to the Tasmanian Gateway, the deep opening of Drake Passage in the Late Oligocene induced strong increase in

the Southern Ocean SST gradient and cooling of Antarctic surface waters, also in the Tasmanian Gateway area. We further conclude that despite the cooling induced by widening Southern Ocean gateways, global ice volume apparently declined in this time interval, likely due to regional Antarctic tectonic changes affecting Antarctic topography and ice mass balance[42], unless there is a low latitude sampling bias in the global benthic foraminiferal $\delta^{18}O$ splice. Although radiative forcing (CO_2, orbital variations) is (likely) the primary driver of the Cenozoic climatic evolution (e.g.[43,47,48]), we here support an important role for paleogeography on Southern Ocean and Antarctic climate.

Conclusion

Our TEX$_{86}$-based SST record from the Oligocene Tasmanian Margin (ODP Site 1168), representing the development of SSTs around the STF, in comparison with the benthic foraminiferal $\delta^{18}O$ splice, pCO$_2$ estimates, regional SST records, and model simulations, show the following:

- The latitudinal SST gradient across the widening AAG was ~6–8 °C in the Late Eocene–Early Oligocene, and increased from 26 Ma, when Antarctic proximal cooling started.
- SST data derived from sediments deposited during glacial or interglacial intervals from the Antarctic proximal site show that the latitudinal SST gradient is larger during glacials. This can be ascribed to the latitudinal migrations of ocean frontal systems, which are limited at the northern boundary of the Southern Ocean by the position of Australia.
- Long term trends in Antarctic ice volume and polar amplification due to decreasing pCO$_2$ cannot alone explain the Antarctic proximal cooling starting at 26 Ma. We correlate this cooling to the first deep opening of Drake Passage which decreased the strength of subpolar ocean gyres and southward heat transport, enhancing Antarctic thermal isolation and circumpolar flow.

Methods

Site description, depositional setting and age model. We reconstruct the changes in sea surface temperature from the subtropical front region by studying marine sediments (766–339 mbsf) from Ocean Drilling Program (ODP) Site 1168 (42°38′40″ S, 144°25′30″ E, present water depth: 2463 m). The site is situated 70 km off the west Tasmanian coast, north of the oceanographic subtropical front, where relatively carbon-rich siliciclastic sediments have filled the graben basin between two basement highs (~25 km length) since the Late Eocene until Early Oligocene and continental slope sedimentation of calcium carbonate-rich sediments thereafter[37,49]. A detailed description of the site location, depositional setting and oceanographic setting has been given in Hoem, et al.[37]. For the age model, we updated ages of tie points interpolated (cf. Stickley, et al.[50]; updated to GTS2012 ages[51] in Hoem, et al.[37]) with the exemption of one last occurrence datum of foraminifera *Subbotina angiporoides*. We interpolated a loess smooth (span of 0.1) through age tie points to obtain the ages of our samples (Supplementary Fig. 1).

TEX$_{86}$ paleothermometry. In order to reconstruct sea surface temperature (SST), we applied the TEX$_{86}$ (TetraEther indeX of 86 carbon atoms) proxy[52], which is based on the temperature-dependent cyclisation of isoprenoidal glycerol dialkyl glycerol tetraethers (GDGTs) produced by thaumarchaeotal membrane lipids. A total of 148 samples spanning the period between 35 and 20 Ma (766–339 mbsf) were processed for analysis of GDGTs (Supplementary Methods; Supplementary Data[32]). GDGTs were extracted from powdered and freeze-dried sediments using a Milestone Ethos X microwave or accelerated solvent extractor system. Lipid extracts were separated into an apolar, ketone and polar fraction by Silica gel column chromatography. GDGT standard was added to the polar fraction and filtered over a 0.45 μm polytetrafluoroethylene filter. The dissolved polar fractions were injected and analysed by high-performance liquid chromatography–mass spectrometry (HPLC–MS) at Utrecht University, using double-column separation[53]. GDGT peaks in the HPLC chromatograms were integrated using ChemStation software. A more detailed description can be found in the Supplementary Methods.

TEX$_{86}$ was calculated as defined by Schouten, et al.[52]:

$$'\text{TEX}_{86}' = \frac{GDGT-2 + GDGT-3 + Cren'}{GDGT-1 + GDGT-2 + GDGT-3 + Cren'}$$

TEX$_{86}$ results were examined for non-thermal overprints (described in detail in Supplementary Methods) to verify the reliability of their SST signal (Supplementary Data[32]; Supplementary Fig. 2–6) and compared to an alkenone-derived ($U^{k'}_{37}$) SST record from the same site[33] (Supplementary Fig. 7). For systematic calculation of GDGT ratios, data analysis, visualization, and evaluation of isoGDGT, brGDGT and/or brGMGT data, we utilized the R script of Bijl, et al.[29]: https://github.com/bijlpeter83/RGDGT.git. We uploaded the measured peak areas (Supplementary Data[32]) of GDGTs in the R script and calculated and plotted fractional abundances, overprinting indices and paleotemperature time series (Supplementary Figs. 2–4).

In order to translate the TEX$_{86}$ values into SSTs, we used the regionally varying, Bayesian; BAYSPAR SST (prior mean of 30 °C, prior standard deviation of 20) of Tierney and Tingley[54] (Supplementary Fig. 5). The BAYSPAR method compares measured TEX$_{86}$ values with similar values in the modern SST observations, obtained from surface sediment samples, to derive linear regression parameters: BAYSPAR propagates uncertainties in the surface sediment data into resulting temperature predictions[54]. SST estimates obtained with the exponential transfer function BAYSPAR are very similar to the TEX$_{86}$-based SSTs produced by the exponential function from Kim, et al.[55] and linear function by O'Brien, et al.[56] (Supplementary Fig. 6), varying, at most, by 2 °C.

Temperature data compilation. We compiled existing Oligocene TEX$_{86}$ data and applied the BAYSPAR SST calibration[54] for consistency, from east of Tasmania: ODP Site 1172[29], north of the Ross Sea: DSDP Site 274[2], offshore Wilkes Land: IODP Site U1356[1] and DSDP Site 269[30]. The age model for the terrestrial temperature records from the Ross Sea: Cape Roberts Project (CRP)[31] based on Lavelle[57], McIntosh[58], and Florindo, et al.[59], was converted to GTS2012 ages[51] for the purpose of this paper.

Fully coupled climate model. For model-data intercomparisons, we utilized a suite of general circulation model (GCM) HadCM3BL-M2.1aE model experiments, with full atmospheric coupling, carried out and described by Kennedy-Asser, et al.[26] and compiled by the Bridge Consortium of the University of Bristol (found at http://www.bridge.bris.ac.uk/resources/simulations). Simulations that were selected for comparison (Fig. 3b) were built using boundary conditions, developed by Getech Group plc, appropriate for Rupelian and Chattian-age paleogeographies with either a closed or open Drake Passage, narrow or wide Tasmanian Gateway, using varying ice sheet constructions (either no ice sheet, East Antarctic Ice Sheet (EAIS) only, or full Antarctic Ice Sheet (AIS)), and varying pCO$_2$ concentrations (either 560 or 1120 ppm) (Supplementary Table 2, Supplementary Figs. 8 and 9). These simulations were used in this study because the model has been extensively applied in the Eocene and Oligocene and extensive sensitivity tests to length of integration, paleogeographic boundary conditions, and pCO$_2$ have been conducted. Although the HadCM3L ocean resolution is low, the influence of an Antarctic ice sheet does not necessitate a high-resolution ocean to a great degree. Furthermore, the lengthy spin-up time of the Kennedy-Asser, et al.[26] experiments help minimize any uncertainty in their results and makes them highly robust for this comparison. As with nearly all coupled climate models, this model tends to require higher greenhouse gas concentrations than is typical of reconstructions to achieve sufficiently warm high latitude temperatures. This is likely a byproduct of a too low value of global equilibrium climate sensitivity as has been widely described previously[60–62]. We are here comparing relative changes, so this systematic bias is not likely to importantly impact the interpretation of our results.

High-resolution eddy-resolving ocean model. The presented high-resolution ocean simulations (Fig. 3c) are taken from Sauermilch, et al.[25]. It uses the Massachusetts Institute of Technology ocean general circulation model (MITgcm)[63] with a circum-Antarctic model domain (from 84°S to 25°S). The spatial resolution is 0.25° (3–25 km resolution) and vertical resolution contains 50 layers (ranging from 10 m at the sea surface to 368 m at the sea floor). Southern Ocean paleogeography is reconstructed to the Late Eocene (38 Ma) position using the plate tectonic model of Matthews, et al.[64] in a paleomagnetic reference frame[65].

The model is ocean-only and atmospheric forcing are taken from a coupled atmosphere-ocean simulation (GFDL CM2.1) run with atmospheric pCO$_2$ concentration of 800 ppm[66]. A restoring time scale of 10 days is applied. Although not directly coupled to the atmosphere or ice sheet, the resolution of the ocean model is higher than most previous paleo-simulations and permits the formation of ocean eddies which are responsible for the majority of the ocean heat transport[67]. The high-resolution model is less diffusive, allowing accurate simulation of subsurface velocities and current structure. In addition, detailed paleobathymetry features such as the seafloor roughness, but also small depth changes in the critical gateway regions, Tasman Gateway and Drake Passage, can be accurately resolved. To accommodate this advantage, new high-resolution paleobathymetry grids are used[68] which are able to reconstruct detailed seafloor roughness features, such as seamounts and fracture zones, that have a substantial impact on the large-scale ocean circulation (e.g. LaCesca, et al.[69]). See Sauermilch, et al.[25] for further details

about the methodology of the high-resolution ocean model and paleobathymetry reconstruction.

Data availability

References

1. Hartman, J. D. et al. Paleoceanography and ice sheet variability offshore Wilkes Land, Antarctica-Part 3: Insights from Oligocene-Miocene TEX86-based sea surface temperature reconstructions. *Clim Past* **14**, 1275–1297 (2018).
2. Hoem, F. S. et al. Temperate Oligocene surface ocean conditions offshore of Cape Adare, Ross Sea, Antarctica. *Clim Past* **17**, 1423–1442 (2021a).
3. Houben, A. J. P., Bijl, P. K., Sluijs, A., Schouten, S. & Brinkhuis, H. Late Eocene Southern Ocean Cooling and Invigoration of Circulation Preconditioned Antarctica for Full-Scale Glaciation. *Geochem Geophys Geosyst* **20**, 2214–2234 (2019).
4. Liu, Z. et al. Global cooling during the eocene-oligocene climate transition. *Science* **323**, 1187–1190 (2009).
5. Bohaty, S. M., Zachos, J. C. & Delaney, M. L. Foraminiferal Mg/Ca evidence for southern ocean cooling across the eocene–oligocene transition. *Earth Planet Sci Lett* **317**, 251–261 (2012).
6. Galeotti, S. et al. Antarctic Ice Sheet variability across the Eocene-Oligocene boundary climate transition. *Science* **352**, 76–80 (2016).
7. Levy, R. H. et al. Antarctic ice-sheet sensitivity to obliquity forcing enhanced through ocean connections. *Nat. Geosci.* **12**, 132–137 (2019).
8. Zachos, J. C., Stott, L. D. & Lohmann, K. C. Evolution of early Cenozoic marine temperatures. *Paleoceanography* **9**, 353–387 (1994).
9. O'Brien, C. L. et al. The enigma of Oligocene climate and global surface temperature evolution. *Proc. Natl. Acad. Sci. U S A* **117**, 25302–25309 (2020).
10. Hoenisch, B. *Paleo-CO2 data archive (Version 1) [Data set]. Zenodo.*, (2021).
11. Gasson, E. et al. Uncertainties in the modelled CO 2 threshold for Antarctic glaciation. *Clim. Past* **10**, 451–466 (2014).
12. Goldner, A., Herold, N. & Huber, M. Antarctic glaciation caused ocean circulation changes at the Eocene–Oligocene transition. *Nature* **511**, 574–577 (2014).
13. Paxman, G. J. et al. Reconstructions of Antarctic topography since the Eocene–Oligocene boundary. *Palaeogeography, palaeoclimatology, palaeoecology* **535**, 109346 (2019).
14. Wilson, D. S. & Luyendyk, B. P. West Antarctic paleotopography estimated at the Eocene-Oligocene climate transition. *Geophys. Res. Lett.* **36** (2009).
15. Bijl, P. K. et al. Paleoceanography and ice sheet variability offshore Wilkes Land, Antarctica-Part 2: Insights from Oligocene-Miocene dinoflagellate cyst assemblages. *Clim. Past* **14**, 1015–1033 (2018).
16. Sangiorgi, F. et al. Southern Ocean warming and Wilkes Land ice sheet retreat during the mid-Miocene. *Nat. commun.* **9**, 317 (2018).
17. Singh, H. K., Bitz, C. M. & Frierson, D. M. The global climate response to lowering surface orography of Antarctica and the importance of atmosphere–ocean coupling. *J. Clim.* **29**, 4137–4153 (2016).
18. Hill, D. J. et al. Paleogeographic controls on the onset of the Antarctic circumpolar current. *Geophys. Res. Lett.* **40**, 5199–5204 (2013).
19. England, M. H., Hutchinson, D. K., Santoso, A. & Sijp, W. P. Ice–atmosphere feedbacks dominate the response of the climate system to Drake Passage closure. *J. Clim.* **30**, 5775–5790 (2017).
20. Evangelinos, D. et al. Absence of a strong, deep-reaching Antarctic Circumpolar Current zonal flow across the Tasmanian gateway during the Oligocene to early Miocene. *Global Planet. Change* **208**, 103718 (2022).
21. Knorr, G. & Lohmann, G. Climate warming during Antarctic ice sheet expansion at the Middle Miocene transition. *Nat. Geosci.* **7**, 376–381 (2014).
22. Kennedy, A. T., Farnsworth, A., Lunt, D., Lear, C. H. & Markwick, P. Atmospheric and oceanic impacts of Antarctic glaciation across the Eocene–Oligocene transition. *Philosophical Transactions of the Royal Society A: Mathematical, Physical and Engineering Sciences* **373**, 20140419 (2015).
23. Westerhold, T. et al. An astronomically dated record of Earth's climate and its predictability over the last 66 million years. *Science* **369**, 1383–1387 (2020).
24. Lear, C. H., Rosenthal, Y., Coxall, H. K. & Wilson, P. Late Eocene to early Miocene ice sheet dynamics and the global carbon cycle. *Paleoceanography* **19**, https://doi.org/10.1029/2004PA001039 (2004).
25. Sauermilch, I. et al. Gateway-driven Southern Ocean cooling – The crucial role of ocean gyres. *Nature Communications* **2021**, https://doi.org/10.1038/s41467-021-26658-1 (2021).
26. Kennedy-Asser, A., Lunt, D. J., Farnsworth, A. & Valdes, P. Assessing mechanisms and uncertainty in modeled climatic change at the Eocene-Oligocene transition. *Paleoceanography Paleoclimatol.* **34**, 16–34 (2019).
27. Sijp, W. P., England, M. H. & Huber, M. Effect of the deepening of the Tasman Gateway on the global ocean. *Paleoceanography* **26** (2011).
28. van de Lagemaat, S. H. et al. Subduction initiation in the Scotia Sea region and opening of the Drake Passage: When and why? *Earth-Science Reviews*, 103551, https://doi.org/10.1016/j.earscirev.2021.103551 (2021).
29. Bijl, P. K. et al. Maastrichtian-Rupelian paleoclimates in the southwest Pacific–a critical evaluation of biomarker paleothermometry and dinoflagellate cyst paleoecology at Ocean Drilling Program Site 1172. *Climate of the Past Discussions*, 1-82 (2021).
30. Evangelinos, D. et al. Late Oligocene-Miocene proto-Antarctic Circumpolar Current dynamics off the Wilkes Land margin, East Antarctica. *Global. Planet. Change* **191**, 103221 (2020).
31. Passchier, S. et al. Early Eocene to middle Miocene cooling and aridification of East Antarctica. *Geochem. Geophys. Geosys.* **14**, 1399–1410 (2013).
32. Bijl, P. K., Hoem, F.S., & Hou, S. Sea-surface temperature proxy data (TEX86 and UK'37) from Ocean Drilling Program Site 1168 [Data set]. https://doi.org/10.5281/zenodo.7119904 (2022).
33. Guitián, J. & Stoll, H. M. Evolution of Sea Surface Temperature in the Southern Mid-latitudes from Late Oligocene through Early Miocene. *Paleoceanography and Paleoclimatology*, e2020PA004199, https://doi.org/10.1029/2020PA004199 (2021).
34. Herbert, T. et al. Depth and seasonality of alkenone production along the California margin inferred from a core top transect. *Paleoceanography* **13**, 263–271 (1998).
35. Rattanasriampaipong, R., Zhang, Y. G., Pearson, A., Hedlund, B. P. & Zhang, S. Archaeal lipids trace ecology and evolution of marine ammonia-oxidizing archaea. *Proc. Natl. Acad. Sci.* **119**, e2123193119 (2022).
36. Van Der Weijst, C. M. et al. A 15-million-year surface-and subsurface-integrated TEX86 temperature record from the eastern equatorial Atlantic. *Climate. Past* **18**, 1947–1962 (2022).
37. Hoem, F. S. et al. Late Eocene–early Miocene evolution of the southern Australian subtropical front: a marine palynological approach. *J. Micropalaeontol.* **40**, 175–193 (2021b).
38. Olbers, D., Borowski, D., Völker, C. & Woelff, J.-O. The dynamical balance, transport and circulation of the Antarctic Circumpolar Current. *Antarctic Sci.* **16**, 439–470 (2004).
39. Valdes, P. J. et al. The BRIDGE HadCM3 family of climate models: HadCM3@ Bristol v1. 0. *Geosci. Model Dev.* **10**, 3715–3743 (2017).
40. Salabarnada, A. et al. Paleoceanography and ice sheet variability offshore Wilkes Land, Antarctica–Part 1: Insights from late Oligocene astronomically paced contourite sedimentation. *Climate Past* **14**, 991–1014 (2018).
41. Barrett, P. Cenozoic climate and sea level history from glacimarine strata off the Victoria Land coast, Cape Roberts Project, Antarctica. *Glacial sedimentary processes and products*, 259-287 (2007).
42. Duncan, B. et al. Climatic and tectonic drivers of late Oligocene Antarctic ice volume. *Nature Geoscience*, 1-7 (2022).
43. Huber, M. et al. Eocene circulation of the Southern Ocean: Was Antarctica kept warm by subtropical waters? *Paleoceanography* (2004).
44. Nicholson, U. & Stow, D. Erosion and deposition beneath the Subantarctic Front since the Early Oligocene. *Sci. Rep.* **9**, 1–9 (2019).
45. Scher, H. D. et al. Onset of Antarctic Circumpolar Current 30 million years ago as Tasmanian Gateway aligned with westerlies. *Nature* **523**, 580–583 (2015).
46. Lyle, M., Gibbs, S., Moore, T. C. & Rea, D. K. Late Oligocene initiation of the Antarctic Circumpolar Current: Evidence from the South Pacific. *Geology* **35**, 691–694 (2007).
47. Hutchinson, D. K. et al. The Eocene–Oligocene transition: a review of marine and terrestrial proxy data, models and model–data comparisons. *Climate Past* **17**, 269–315 (2021).
48. Cramwinckel, M. J. et al. Synchronous tropical and polar temperature evolution in the Eocene. *Nature* **559**, 382–386 (2018).
49. Exon, N. F., et al.,. Site 1168. *Proceedings of the Ocean Drilling Program Initial Reports, Ocean Drilling Program, College Station, TX., USA*, (2001).
50. Stickley, C. et al. in *Proceedings of the Ocean Drilling Program, Scientific Results*. 1-57 (Ocean Drilling Program, College Station TX).
51. Gradstein, F. M., Ogg, J. G., Schmitz, M. D. & Ogg, G. M. *The geologic time scale 2012*. (elsevier, 2012).
52. Schouten, S., Hopmans, E. C., Schefuß, E. & Damste, J. S. S. Distributional variations in marine crenarchaeotal membrane lipids: a new tool for reconstructing ancient sea water temperatures? *Earth Planet. Sci. Lett.* **204**, 265–274 (2002).

53. Hopmans, E. C., Schouten, S. & Damsté, J. S. S. The effect of improved chromatography on GDGT-based palaeoproxies. *Organic Geochemistry* **93**, 1–6 (2016).

54. Tierney, J. E. & Tingley, M. P. A TEX 86 surface sediment database and extended Bayesian calibration. *Sci. data* **2**, 1–10 (2015).

55. Kim, J.-H. et al. New indices and calibrations derived from the distribution of crenarchaeal isoprenoid tetraether lipids: Implications for past sea surface temperature reconstructions. *Geochimica et Cosmochimica Acta* **74**, 4639–4654 (2010).

56. O'Brien, C. L. et al. Cretaceous sea-surface temperature evolution: Constraints from TEX86 and planktonic foraminiferal oxygen isotopes. *Earth-Sci. Rev.* **172**, 224–247 (2017).

57. Lavelle, M. Strontium isotope stratigraphy of the CRP-1 drillhole, Ross Sea, Antarctica. *Terra Antartica* **5**, 691–696 (1998).

58. McIntosh, W. 40Ar/39Ar geochronology of volcanic clasts and pumice in CRP-1 core, Cape Roberts, Antarctica. *Terra Antartica* **5**, 683–690 (1998).

59. Florindo, F., Wilson, G. S., Roberts, A. P., Sagnotti, L. & Verosub, K. L. Magnetostratigraphic chronology of a late Eocene to early Miocene glacimarine succession from the Victoria Land Basin, Ross Sea, Antarctica. *Global Planet. Change* **45**, 207–236 (2005).

60. Caballero, R. & Huber, M. State-dependent climate sensitivity in past warm climates and its implications for future climate projections. *Proc. Natl. Acad. Sci.* **110**, 14162–14167 (2013).

61. Lunt, D. J. et al. A model–data comparison for a multi-model ensemble of early Eocene atmosphere–ocean simulations: EoMIP. *Clim. Past* **8**, 1717–1736 (2012).

62. Hansen, J., Sato, M., Russell, G. & Kharecha, P. Climate sensitivity, sea level and atmospheric carbon dioxide. *Philos. Trans. Royal Society A: Mathe. Phys. Eng. Sci.* **371**, 20120294 (2013).

63. Marshall, J., Adcroft, A., Hill, C., Perelman, L. & Heisey, C. A finite-volume, incompressible Navier Stokes model for studies of the ocean on parallel computers. *J. Geophys. Res.: Oceans* **102**, 5753–5766 (1997).

64. Matthews, K. J. et al. Global plate boundary evolution and kinematics since the late Paleozoic. *Global Planet. Chan.* **146**, 226–250 (2016).

65. van Hinsbergen, D. J. et al. A paleolatitude calculator for paleoclimate studies. *PloS ONE* **10**, e0126946 (2015).

66. Hutchinson, D. K. et al. Climate sensitivity and meridional overturning circulation in the late Eocene using GFDL CM2. 1. *Clim. Past* **14**, 789–810 (2018).

67. Viebahn, J. P., von der Heydt, A. S., Le Bars, D. & Dijkstra, H. A. Effects of Drake Passage on a strongly eddying global ocean. *Paleoceanography* **31**, 564–581 (2016).

68. Hochmuth, K. et al. The evolving paleobathymetry of the circum-Antarctic Southern Ocean since 34 Ma: A key to understanding past cryosphere-ocean developments. *Geochem. Geophys. Geosyst.* **21**, e2020GC009122 (2020).

69. Lacasce, J. H., Escartin, J., Chassignet, E. P. & Xu, X. Jet instability over smooth, corrugated, and realistic bathymetry. *J. Phys. Oceanography* **49**, 585–605 (2019).

70. Müller, R. D. et al. GPlates: building a virtual Earth through deep time. *Geochem. Geophys. Geosyst.* **19**, 2243–2261 (2018).

Author contributions
P.K.B. and F.S. designed the research. F.S.H. conducted the research and wrote the paper with input from all co-authors. P.K.B. converted the age model to the GTS2012 timescale. F.S.H. requested, processed and integrated samples for TEX_{86} paleothermometry. F.S.H., P.K.B., F.S. and F.P. interpreted the TEX_{86}-SST data. IS made the high-resolution the ocean model simulation. A.K.A. and M.H. made the fully coupled general circulation model simulation. All co-authors approve the manuscript and agrees to its submission.

Competing interests
The authors declare no competing interests.

Additional information
Supplementary information The online version contains supplementary material available at https://doi.org/10.1038/s43247-022-00666-5.

Correspondence and requests for materials should be addressed to Frida S. Hoem.

Peer review information *Communications Earth & Environment* thanks Zhonghui Liu, Tom Dunkley Jones and the other, anonymous, reviewer(s) for their contribution to the peer review of this work. Primary Handling Editors: Sze Ling Ho, Joe Aslin. Peer reviewer reports are available.

Reprints and permission information is available at http://www.nature.com/reprints

Publisher's note Springer Nature remains neutral with regard to jurisdictional claims in published maps and institutional affiliations.